



HAL
open science

Modeling of a Remote Center of Motion Spherical Parallel Tensegrity Mechanism for Percutaneous Interventions

Hamza El Jjouaoui, Giorgio Mackenzie Cruz-Martinez, Juan Carlos Avila Vilchis, Adriana Herlinda Vilchis-Gonzalez, Salih Abdelaziz, Philippe Poignet

► To cite this version:

Hamza El Jjouaoui, Giorgio Mackenzie Cruz-Martinez, Juan Carlos Avila Vilchis, Adriana Herlinda Vilchis-Gonzalez, Salih Abdelaziz, et al.. Modeling of a Remote Center of Motion Spherical Parallel Tensegrity Mechanism for Percutaneous Interventions. ARK 2022 - 18th International Symposium on Advances in Robot Kinematics, Jun 2022, Bilbao, Spain. pp.332-339, 10.1007/978-3-031-08140-8_36 . hal-04565727

HAL Id: hal-04565727

<https://hal.science/hal-04565727v1>

Submitted on 2 May 2024

HAL is a multi-disciplinary open access archive for the deposit and dissemination of scientific research documents, whether they are published or not. The documents may come from teaching and research institutions in France or abroad, or from public or private research centers.

L'archive ouverte pluridisciplinaire **HAL**, est destinée au dépôt et à la diffusion de documents scientifiques de niveau recherche, publiés ou non, émanant des établissements d'enseignement et de recherche français ou étrangers, des laboratoires publics ou privés.

Modeling of a Remote Center of Motion Spherical Parallel Tensegrity Mechanism for Percutaneous Interventions

H. El Jjouaoui, G. Cruz-Martinez, J-C. Avila Vilchis, A. Vilchis González, S. Abdelaziz and P. Poignet

Abstract The present paper deals with the mathematical modeling of a new 2 DOF remote center of motion spherical parallel tensegrity mechanism, dedicated to percutaneous needle interventions. Analytical inverse kinematic and numerical direct kinematic models are developed. Trilateration approach is considered in order to determine the coordinates of the joints that constitute the system. A 3D prototype of the mechanism has been developed for future evaluations. This work constitutes a first step towards the control of the mechanism.

Key words: Spherical RCM parallel structure, tensegrity system, Modeling

1 Introduction

In Interventional radiology, needle puncture is widely used for cancer diagnosis and treatment, such as biopsy and ablation [1]. To perform these gestures, it is necessary to manually adjust the needle position and orientation. Feedback from imagers (MRI, CT, US) [2] is necessary to determine the exact position of the needle. Using a robotic assistant instead of radiologist's hand to position the needle is of interest since it increases the needle position accuracy [3] [4].

Using a tensegrity architecture to design a robotic assistant is of great interest, particularly when stiffness variation is required [5]. Tensegrity structures were introduced for the first time by Richard B. Fuller [6]. They can be defined as structures composed of rigid compressed elements (bars) forming a self-equilibrium that preserve its stable state using the forces produced by the tension of flexible elements (springs, cables) that are linked to the rigid parts [7]. Designing a robot based on

Hamza El Jjouaoui
LIRMM, France, e-mail: hamza.el-jjouaoui@lirmm.fr

Salih Abdelaziz
LIRMM, France, e-mail: salih.abdelaziz@lirmm.fr

tensegrity allows to produce efficient structures [8] with variable stiffness, high precision as well as high volume-to-mass ratio and stiffness-to-mass ratio [9].

The main challenge for such robotized medical interventions is to design a remote center of motion (RCM) mechanism that allows a rotational movement around a fixed point, which is in our case the needle insertion point. There are several mechanism architectures in the literature that guarantee a rotation around a RCM [10]. Our approach is based on the use of a spherical parallel RCM [11] that is redesigned to incorporate the concept of tensegrity. Pantographs, constituted by rigid curved bars, are introduced to the mechanism. These bars are connected to each other using revolute joints. The joints axis are directed towards the RCM [12]. The pantographs have the form of spherical parallelograms that allow the incorporation of cables and springs to define the system as a spherical remote center of motion tensegrity mechanism. It is a 2 DOF mechanism driven by 4 cables. The 2 degrees of redundancy are used to vary the stiffness of the mechanism.

This work deals with the kinematic modeling of such a system. In section 2, the system description is introduced. In section 3, the inverse and the direct kinematic models as well as the workspace estimation are derived. The trilateration approach that allows the computation of the joints coordinates is also introduced. Finally, conclusions and perspectives are discussed in section 4.

2 System Description

The system, as illustrated in Fig. 1, is a spherical RCM mechanism. The needle guide is the end effector of the mechanism. It is manipulated using two spherical pantographs. The first pantograph is located in a sphere surface of radius R_1 . It is connected to the base at the joint A_1 . Similarly, the second pantograph is located in a sphere surface of radius R_2 and is connected to the base at the joint A_2 . The manipulation of each pantograph is obtained by manipulating a pair of two cables. The first cable is attached to the joint B_1 , passes through a pulley located at D_1 and some other pulleys before being winded on a first actuated pulley. The second cable is attached to the joint C_1 , passes through a pulley located at A_1 and some other pulleys before being winded on the second actuated pulley. Similarly, the second pantograph is manipulated using two actuated cables 3 and 4.

3 System Modeling

The origin of the reference frame $\mathcal{R}_0 = (O, \mathbf{x}_0, \mathbf{y}_0, \mathbf{z}_0)$ is defined as the RCM of the mechanism (Fig. 1). The end effector orientation is defined by $\mathbf{x} = [\eta \ \mu]^T$ (Fig. 2, left). The coordinates of the joint T are expressed in the reference frame \mathcal{R}_0 as $\mathbf{T} = [T_x \ T_y \ T_z]^T$. The joint variables are defined by $\boldsymbol{\beta} = [\beta_1 \ \beta_2]^T$. The variable β_i represents the angle between $(A_i B'_i)$ and $(A_i D'_i)$. The points B'_i and D'_i represent

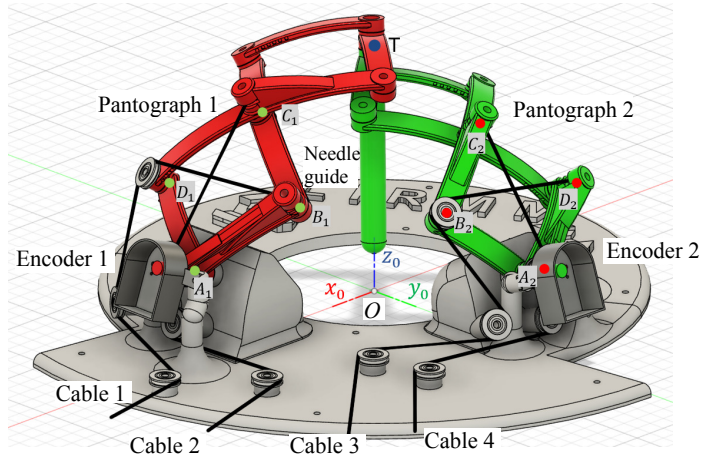


Fig. 1 System overview.

respectively the projection of the points B_i and D_i on the plane (P_1) (Fig. 2, right). These joint variables are measured using optical encoders located at the joints A_1 and A_2 (Fig. 1).

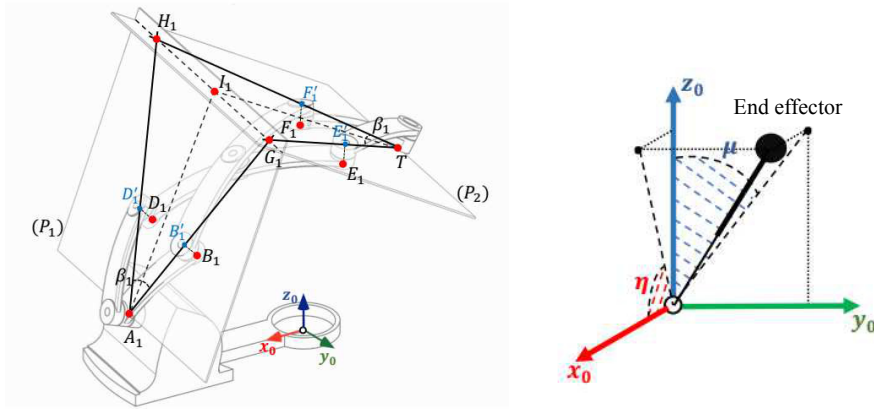


Fig. 2 Right, joint variables definition. Left, end effector orientation.

3.1 Inverse Kinematic Model

The inverse kinematic (IK) model allows to express the joint variables $\boldsymbol{\beta} = [\beta_1 \ \beta_2]^T$ according to the orientation $\mathbf{x} = [\eta \ \mu]^T$ of the needle guide. This orientation is supposed to be known and can be expressed using the coordinates of $\mathbf{T} = [T_x \ T_y \ T_z]^T$. The IK model is determined in two steps. First, a relationship between β_i and θ_i is established. θ_i represents the angle between (OT) and (OA_i) (Fig. 3). In the second step, a relationship between the angle θ_i and the end effector position \mathbf{T} is derived.

From Fig. 2, right, one can notice that $\|A_1 I_1\| = f_1 \cos(\beta_1/2)$ where $f_1 = \|A_1 G_1\|$. The distance f_1 is fixed whereas $\|A_1 I_1\|$ is variable. This latter can be used to compute the distance $\|A_1 K_1\| = \|A_1 I_1\| \cos(\theta_1/2)$, as it can be observed from Fig.3. Besides, $\|A_1 K_1\| = R_1 \sin(\theta_1/2)$. Based on these 3 equations, one can express the relationship between β_1 and θ_1 , and similarly the relationship between β_2 and θ_2 for the second pantograph:

$$\beta_i = 2 * \cos^{-1}(R_i / f_i * \tan(\theta_i/2)) \quad (1)$$

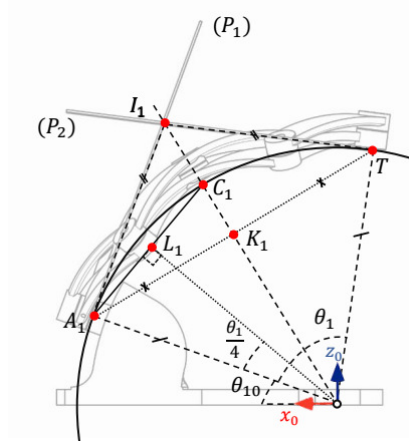


Fig. 3 Definition of the relationship between θ_1 and β_1

Knowing the coordinates of the vectors \mathbf{T} , \mathbf{A}_1 and \mathbf{A}_2 , it is possible to compute the angle θ_1 between \mathbf{T} and \mathbf{A}_1 , and the angle θ_2 between \mathbf{T} and \mathbf{A}_2 :

$$\begin{cases} \theta_1 = \pm \cos^{-1} \left(\frac{\mathbf{A}_1^T \mathbf{T}}{\|\mathbf{A}_1\| \|\mathbf{T}\|} \right) = \pm \cos^{-1} \left(\frac{T_x \cos(\theta_{10}) + T_z \sin(\theta_{10})}{R_1} \right) \\ \theta_2 = \pm \cos^{-1} \left(\frac{\mathbf{A}_2^T \mathbf{T}}{\|\mathbf{A}_2\| \|\mathbf{T}\|} \right) = \pm \cos^{-1} \left(\frac{T_y \cos(\theta_{20}) + T_z \sin(\theta_{20})}{R_1} \right) \end{cases} \quad (2)$$

where θ_{10} is the angle between (OA_1) and \mathbf{x}_0 axis and θ_{20} is the angle between (OA_2) and \mathbf{y}_0 axis. Only positive solutions are considered since the robot can evolve only in the upper hemisphere.

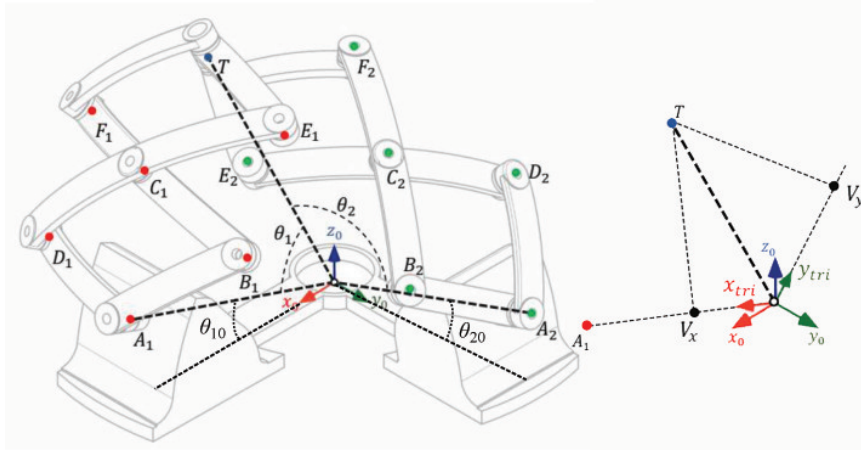


Fig. 4 Robot parametrization.

3.2 Direct Kinematic Model

The direct kinematic allows to express the orientation of the needle guide $\mathbf{x} = [\eta \ \mu]^T$ according to the joint variables $\boldsymbol{\beta} = [\beta_1 \ \beta_2]^T$. This is performed also in two steps. First, the relationship between θ_i and β_i is established by inverting (1):

$$\theta_i = 2 * \tan^{-1}(f_i/R_i * \cos(\beta_i/2)) \quad (3)$$

The second step consists in solving the following system of equations, obtained by inverting (2):

$$\begin{cases} T_x \cos(\theta_{10}) + T_z \sin(\theta_{10}) - R_1 \cos(\theta_1) = 0 \\ T_y \cos(\theta_{20}) + T_z \sin(\theta_{20}) - R_1 \cos(\theta_2) = 0 \\ T_x^2 + T_y^2 + T_z^2 - R_1^2 = 0 \end{cases} \quad (4)$$

This system of equation could possibly be solved analytically but here a numerical approach is considered. Finally, the end effector orientations are computed by:

$$\begin{aligned} \eta &= \text{atan2}(T_y, T_z) \\ \mu &= \text{atan2}(T_z, T_x) \end{aligned} \quad (5)$$

To determine the coordinates of the joints B_i , C_i , D_i , E_i and F_i in the reference frame \mathcal{R}_0 (Fig. 4), a trilateration approach is considered. This approach is based on the intersection of 3 known spheres to determine the coordinates of the intersection point. In the following, we will show how to determine the coordinates of C_1 and the same approach can be considered to determine the coordinates of the other joints.

The three spheres that are used to determine the coordinates of C_1 are (S1), (S2) and (S3). (S1) has O as the origin and $r_1 = R_1$ as a radius. (S2) has the coordinates of A_1 as a center and $r_2 = \|A_1 C_1\|$ as a radius. (S3) has the coordinates of T as a center and $r_3 = \|A_1 C_1\|$ as a radius. The distance $\|A_1 C_1\|$ is computed as $\|A_1 C_1\| = 2R_1 \sin(\theta_1/4)$ (Fig.3). The spheres are defined as:

A trilateration frame $\mathcal{R}_{tri} = (O, \mathbf{x}_{tri}, \mathbf{y}_{tri}, \mathbf{z}_{tri})$ is defined. The \mathbf{x}_{tri} axis is chosen along A_1 . The axis \mathbf{y}_{tri} is chosen so that T is in the plane $(\mathbf{x}_{tri} \mathbf{y}_{tri})$:

$$\begin{cases} \mathbf{x}_{tri} = \mathbf{A}_1 / \|\mathbf{A}_1\| \\ \mathbf{z}_{tri} = \mathbf{T} \times \mathbf{x}_{tri} / \|\mathbf{T} \times \mathbf{x}_{tri}\| \\ \mathbf{y}_{tri} = \mathbf{z}_{tri} \times \mathbf{x}_{tri} \end{cases} \quad (6)$$

where \mathbf{A}_1 represents the vector of coordinates of A_1 in the reference frame. The equation of spheres are:

$$\begin{cases} x^2 + y^2 + z^2 = r_1^2 \\ (x - U)^2 + y^2 + z^2 = r_2^2 \\ (x - V_x)^2 + (y - V_y)^2 + z^2 = r_3^2 \end{cases} \quad (7)$$

where V_x and V_y are the coordinates of T in the trilateration frame. They are computed as $V_x = \mathbf{T}^T \mathbf{x}_{tri}$ and $V_y = \mathbf{T}^T \mathbf{y}_{tri}$. The variable $U = R_1$ represents the coordinate of A_1 in \mathcal{R}_{tri} . The coordinates of C_1 in the trilateration frame \mathcal{R}_{tri} can be computed analytically by solving (7). Finally, the coordinates of C_1 in the reference frame are computed as ${}^0x \ {}^0y \ {}^0z]^T = [\mathbf{x}_{tri} \ \mathbf{y}_{tri} \ \mathbf{z}_{tri}] [x \ y \ z]^T$.

3.3 workspace

The geometric workspace of the robot is depicted in Fig. 5. It has been obtained by varying the joint variables $\beta_i \in [0, \pi]$. The geometric parameters of the robot (Fig. 5) have been chosen so that the obtained workspace covers a required workspace defined as a 40° cone with its head pointing to the RCM.

3.4 prototype

A prototype of the robot has been developed using 3D printing. 2 incremental rotary optical encoders with a resolution of 500 CPR have been integrated in A_1 and A_2 .

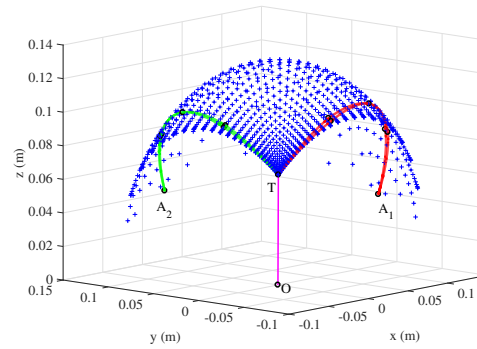


Fig. 5 Geometric workspace obtained using these parameters: $R_1 = 133.9 \text{ mm}$, $R_2 = 133.5 \text{ mm}$, $f_1 = 200 \text{ mm}$, $f_2 = 181.6 \text{ mm}$

The overall structure has 1100 g weight and a volume similar to a hemisphere of approximately 7.8 dm^3 .

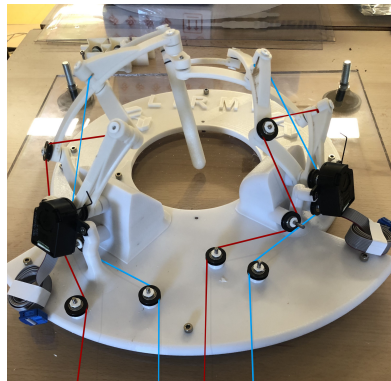


Fig. 6 Prototype of the mechanism.

4 Conclusion and perspectives

A robotic assistant for percutaneous interventions based on spherical RCM tensegrity mechanism has been proposed in this paper. A geometric approach to determine the inverse and direct kinematic models have been developed. The geometric workspace of the robot is shown as a result of the approach, and a prototype has been mounted for

future evaluations. Future work will deal with the differential kinematic modeling, singularity analysis as well as static model determination that are necessary to control the mechanism. Besides and as observed in the actual prototype, structural improvements have to be performed to enhance the vertical stiffness of the robot for a robust manipulation and a better guarantee of the RCM constraint.

References

1. M. Hadavand, M. D. Naish and R. V. Patel, "A parallel Remote Center of Motion mechanism for needle-based medical interventions", 5th IEEE RAS/EMBS International Conference on Biomedical Robotics and Biomechatronics, pp.1-6, 2014.
2. P. Kulkarni, S. Sikander, P. Biswas, S. Frawley, and S.-E. Song, "Review of robotic needle guide systems for percutaneous intervention", *Annals of biomedical engineering*, pp. 1–25, 2019.
3. Y. Wang et al., "Experimental study of the optimum puncture pattern of robot-assisted needle insertion into hyperelastic materials", *Proceedings of the Institution of Mechanical Engineers, Journal of Engineering in Medicine*, 235(1), pp. 28–43. 2021.
4. J. Guo, Yi. Liu, J. Wang, C. Zeng, J. Huang and C. Liu, "The Design of Compact Robotic-Assisted Needle Position System with MPC-Based Remote Control", *Complexity*, pp. 1-13, 2020.
5. J. R. J. Realpe, G. Aiche, S. Abdelaziz and P. Poignet, "Asynchronous and decoupled control of the position and the stiffness of a spatial RCM tensegrity mechanism for needle manipulation", *IEEE International Conference on Robotics and Automation*, pp. 3882-3888, 2020.
6. B. Fuller (ed.), "Synergetics, explorations in the geometry of thinking", Collier Macmillan, 1975.
7. Y. Z. Jing, Ohsaki, M. (eds.): *Tensegrity Structures Form, Stability and Symmetry*. Springer(2015). DOI 10.1007/978-4-431-54813-3.
8. S. H. Juan and J. M. Mirats Tur, "Tensegrity frameworks: Static analysis review", *Mechanism and Machine Theory*, 43(7), pp. 859-881, 2008.
9. S. D. Guest, The stiffness of tensegrity structures, *IMA Journal of Applied Mathematics*, 76(1), pp. 57–66, 2011.
10. S. Aksungur, "Remote Center of Motion (RCM) Mechanisms for Surgical Operations", *International Journal of Applied Mathematics, Electronics and Computers*. 3(2), 2015.
11. S. Bai, "Optimum design of spherical parallel manipulators for a prescribed workspace", *Mechanism and Machine Theory*, pp. 200-211, 2010.
12. A. Molaei, E. Abedloo, H. D. Taghirad, and Z. Marvi, "Kinematic and workspace analysis of diamond: An innovative eye surgery robot", 23rd Iranian Conference on Electrical Engineering, pp. 882–887, 2015.
13. R. E. Skelton and M. C. De Oliveira, "Tensegrity Systems", Springer, 2009.
14. L. Yixiang, B. Qing, Y. Xiaoming, W. Jiang, Y. Bin and L. Yibin, "A review on tensegrity structures-based robots", *Mechanism and Machine Theory*, pp. 104571, 2022
15. M. Arsenault, C. M. Gosselin, "Kinematic, Static, and Dynamic Analysis of a Spatial Three-Degree-of-Freedom Tensegrity Mechanism", *Journal of Mechanical Design*, 128(5), pp. 951-966, 2006.
16. Ji, Zhifei, Li, Tuanjie, Lin, Min., "Kinematics, Singularity, and Workspaces of a Planar 4-Bar Tensegrity Mechanism. *Journal of Robotics*. 2014.
17. J.Kaufman and M.Lee, "Vascular and Interventional Radiology", the Requisites, Mosby Ed., 2004.